Adding Adaptable Stiffness Joints to CPG-Based Dynamic Bipedal Walking Generates Human-Like Gaits

Yan Huang, Yue Gao, Baojun Chen, Qining Wang*, and Long Wang

Intelligent Control Laboratory, College of Engineering,
Peking University, Beijing 100871, China
qiningwang@pku.edu.cn

Abstract. In this paper, we propose a seven-link passivity-based dynamic walking model, in order to further understand the principles of real human walking and provide guidance in building bipedal robots. The model includes an upper body, two thighs, two shanks, flat feet and compliant joints. A bio-inspired central pattern generator (CPG)-based control method is applied to the proposed model. In addition, we add adaptable joint stiffness to the motion control. To validate the effectiveness of the proposed bipedal walking model, we carried out simulations and human walking experiments. Experimental results indicate that human-like walking gaits with different speeds and walking pattern transitions can be realized in the proposed locomotor system.

Keywords: Passive dynamic walking, adaptable stiffness joints, central pattern generators, walking speed control, walking pattern transition.

1 Introduction

Stable bipedal walking is one of the most important components of humanoid robot design, which can help us better understand human natural walking. Compared with bipedal walking based on trajectory-control methods [1], which are commonly applied in industrial robots, passive dynamic walking pioneered by McGeer [2] shows more natural gaits and more efficient motions [3]. In order to understand motion characteristics of passive walkers with more natural anthropomorphic features, researchers have added the upper body [4], knee joints [5], feet with different shapes [6, 7] and compliant ankle joints [8–10]. Although passivity-based walkers can achieve higher energetic efficiency, they have limitations of practical uses [11].

Variable joint stiffness attracted increasing attention in passivity-based walking community, to improve the motion adaptability and versatility. In human walking gaits, joint stiffness plays as an energy-conserving mechanism [12]. The elastic elements of muscles absorb and release mechanical energy alternatively in each step and the adaptivity and efficiency can be improved [9]. Several studies analyzed the effects of the ankle stiffness on motion characteristics of flat-foot dynamic walkers [9, 13]. Owaki *et al.* added hip torsional spring and leg springs to a two-link passive bipedal model and obtain multiple gaits with different stiffness [14]. Our previous studies indicated the

* Corresponding author.

J.-H. Kim et al. (eds.), *Robot Intelligence Technology and Applications 2*,
Advances in Intelligent Systems and Computing 274,
DOI: 10.1007/978-3-319-05582-4_49, © Springer International Publishing Switzerland 2014

important effects of ankle compliance on gait selection [10] and realized speed and step length control of bipedal walkers with adaptable joint stiffness [15]. However, few efforts have been made in systematic control methods in variable-joint-stiffness bipeds and the comparison between the control performance and human natural gaits.

A variety of central pattern generator (CPG) models have been designed and applied to locomotion control of passivity-based bipedal walkers [16–18]. Several studies have reported evidences of the existence of CPG in vertebrates [19, 20]. Previous studies indicated that the biologically inspired CPG-based control methods could enhance robustness against perturbations, improve efficiency, and modulate complex motion behaviors by receiving only a few input signals [21].

In this paper, we propose a human-like passivity-based dynamic walking model with adaptable joint stiffness and CPGs for motion control. The model consists of an upper body, two thighs, two shanks and flat feet. The CPG models reduce the control parameters and simplify the control structure in a natural way. In most existing studies on CPG-controlled bipedal walking, the higher center generates only one driven signal for adjusting the basic rhythm of joint torques and controlling walking behavior [16–18]. The novelty of this study is introducing real-time stiffness control to the CPG-based control system, which shows great resemblance with natural human walking. Through simulations, the locomotion with different motion cycles is studied and the effects of control parameters on walking performance are investigated. In addition, we measure the kinematic data of human normal walking and gait transitions by the 3D human motion capture system. Comparison of the proposed bipedal walking with human gaits shows that our locomotor system can produce human-like gaits and gait transitions. The proposed system may help understand the principles of human normal walking and provide guidance in building efficient and practical bipedal robots.

The rest of this paper is organized as follows. In Section 2, we describe the mechanical and control systems of the seven-link bipedal walking model and depict the protocol of human walking experiments. Section 3 shows the results from both simulation model and human experiments. We conclude in Section 4.

2 Method

2.1 Bipedal Walking Model

We developed a seven-link bipedal walking model, which consists of an upper body, two thighs, two shanks and two flat feet. Each leg includes a hip joint, a knee joint and an ankle joint. The joint stiffness is modeled as a torsional spring at each joint. Thus the control parameters of the mechanical system are all the equilibrium positions and spring constants, which determine the torque and stiffness of each joint. The proposed bipedal walker travels forward on level ground. Fig. 1 shows the structure and the related variables of the bipedal model. A kinematic coupling has been added at the hip to keep the upper body midway between the two thighs. The knee joint is released in push-off and locked when the shank swings to the direction same to the thigh.

Different from a lot of existing passivity-based bipedal walking models with round feet or point feet, flat-foot walkers have the ability of standing stably and more complex walking phase sequences [10]. When the flat foot strikes the ground, there are two

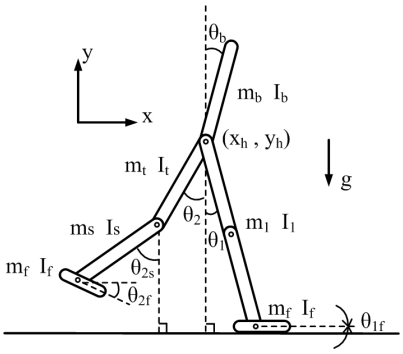

Fig. 1. The passivity-based dynamic bipedal walking model with compliant joints. To simplify the motion, we make the assumptions: 1) the upper body, the legs and the feet are modeled as rigid sticks without flexible deformation; 2) the mass of each part is averagely distributed among the corresponding stick; 3) the friction between the walker and the ground is sufficient. Thus the flat feet do not deform or slip; 4) all strikes are modeled as instantaneous, fully inelastic impacts where no slip and no bounce occurs.

impulses, "heel-strike" and "foot-strike", representing the initial impact of the heel and the following impact as the whole foot contacts the ground, respectively.

The Equation of Motion (EoM) of the proposed bipedal walking model can be obtained by using Lagrange's equation of the first kind. We suppose that the x-axis is along the forward direction while the y-axis is vertical to the ground upwards, as indicated in Fig. 1. The configuration of the walker is defined by the position of the hip joint and the angle of each stick. Thus the posture of the model can be arranged in a generalized vector $\mathbf{q} = (x_h, y_h, \theta_1, \theta_2, \theta_b, \theta_{2s}, \theta_{1f}, \theta_{2f})'$. The superscript $'$ means the transposed matrix (the same in the following paragraphs). The positive directions of all the angles are counter-clockwise. Note that the dimension of the generalized vector in different phases may be different. When the knee joint of the swing leg is locked, the freedom of the shank is reduced and the angle θ_{2s} is not included in the generalized coordinates. Consequently, the dimensions of the mass matrix and the generalized active force are also reduced in some phases.

The model can be defined by the Euclidean coordinates $\mathbf{r}$, which can be described by the x-coordinate and y-coordinate of the center of mass (CoM) of each stick and the corresponding directions. The walker can also be described by the generalized coordinates $\mathbf{q}$ as mentioned before:

$$\mathbf{q} = (x_h, y_h, \theta_1, \theta_2, \theta_b, \theta_{2s}, \theta_{1f}, \theta_{2f})' \tag{1}$$

We defined matrix J as follows:

$$J = d\mathbf{r}/d\mathbf{q} \tag{2}$$

Thus the Jacobian matrix J transfers the generalized velocity $\dot{\mathbf{q}}$ into the velocity of the euclidean coordinates $\dot{\mathbf{x}}$. The mass matrix in rectangular coordinate $\mathbf{r}$ is defined as:

$$M = diag(m_l, m_l, I_l, m_t, m_t, I_t, m_b, m_b, I_b, \\ m_s, m_s, I_s, m_f, m_f, I_f, m_f, m_f, I_f) \tag{3}$$

where m-components are the masses of each stick, while I-components are the moments of inertia, as shown in Fig. 1(a).

The constraint function is marked as $\xi(\mathbf{q})$, which is used to maintain foot contact with ground, the direction of the upper body and locking at the stretched knee joint. Note that $\xi(\mathbf{q})$ in different walking phases may be different since the constraint conditions change. Each component of $\xi(\mathbf{q})$ should keep zero to satisfy the constraint conditions. Each element of the constraint function corresponds to the generalized constrain force.

Then we can obtain the EoM as follows:

$$M_q \ddot{\mathbf{q}} = \mathbf{F_q} + \Phi' \mathbf{F_c} \tag{4}$$

$$\xi(\mathbf{q}) = \mathbf{0} \tag{5}$$

where $\Phi = \frac{\partial \xi}{\partial \mathbf{q}}$. $\mathbf{F_c}$ is the constraint force vector. M_q is the mass matrix in the generalized coordinates:

$$M_q = J' M J \tag{6}$$

$\mathbf{F_q}$ is the active external force in the generalized coordinates:

$$\mathbf{F_q} = J' \mathbf{F} - J' M \frac{\partial J}{\partial \mathbf{q}} \dot{\mathbf{q}} \dot{\mathbf{q}} \tag{7}$$

where $\mathbf{F}$ is the active external force vector in the Euclidean coordinates. For the walking model in this paper, $\mathbf{F}$ includes gravitation, the damping torques, and the joint torques generated by the torsional springs.

Equation (5) can be transformed to the followed equation:

$$\Phi \ddot{\mathbf{q}} = -\frac{\partial (\Phi \dot{\mathbf{q}})}{\partial \mathbf{q}} \dot{\mathbf{q}} \tag{8}$$

Then the EoM in matrix format can be obtained from Equation (4) and Equation (8):

$$\begin{bmatrix} M_q & -\Phi' \\ \Phi & 0 \end{bmatrix} \begin{bmatrix} \ddot{\mathbf{q}} \\ \mathbf{F_c} \end{bmatrix} = \begin{bmatrix} \mathbf{F_q} \\ -\frac{\partial (\Phi \dot{\mathbf{q}})}{\partial \mathbf{q}} \dot{\mathbf{q}} \end{bmatrix} \tag{9}$$

The equation of the strike moment can be obtained by integration of Equation (4):

$$M_q \dot{\mathbf{q}}^+ = M_q \dot{\mathbf{q}}^- + \Phi' \Lambda_c \tag{10}$$

where $\dot{\mathbf{q}}^+$ and $\dot{\mathbf{q}}^-$ are the generalized velocities just after and just before the strike, respectively. Here, Λ_c is the impulse acted on the walker which is defined as follows:

$$\Lambda_c = \lim_{t^- \to t^+} \int_{t^-}^{t^+} \mathbf{F_c} dt \tag{11}$$

Since the strike is modeled as a fully inelastic impact, the walker satisfies the constraint function $\xi(\mathbf{q})$. Thus the motion is constrained by the followed equation after the strike:

$$\frac{\partial \xi}{\partial \mathbf{q}} \dot{\mathbf{q}}^{+} = \mathbf{0} \tag{12}$$

Then the equation of strike in matrix format can be derived from Equation (10) and Equation (12):

$$\begin{bmatrix} M_q & -\Phi' \\ \Phi & 0 \end{bmatrix} \begin{bmatrix} \dot{\mathbf{q}}^{+} \\ \Lambda_c \end{bmatrix} = \begin{bmatrix} M_q \dot{\mathbf{q}}^{-} \\ \mathbf{0} \end{bmatrix} \tag{13}$$

2.2 CPG-Based Control Method

Central Pattern Generators (CPGs) are seemed as neural circuits which can produce coordinated patterns of high-dimensional rhythmic output signals while receiving only simple, low-dimensional, input signals [21]. Thus bio-inspired CPG-based control methods are very suitable for controlling bipedal robots with adaptable stiffness and walking pattern transitions. In this paper, we introduce real-time stiffness control to CPG. The CPG model controls not only the joint torque but also the joint stiffness, which is different from most existing studies on CPG-controlled bipedal walking [16–18]. Thus the natural dynamics of our model can be controlled by adjusting joint stiffness.

The input of the control system in this study is the desired walking pattern while the outputs (i.e. the commands sent to musculo-skeletal system) are joint torque and joint stiffness. The control system receives feedbacks from the motion states of the walker

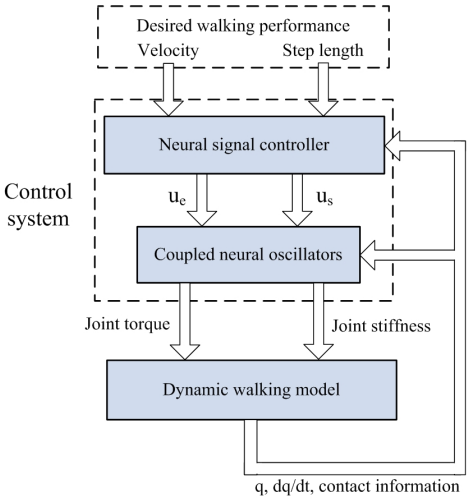

Fig. 2. The diagram of the control scheme. The control system receives the expected walking performance and sends commands as joint torque and joint stiffness to the mechanical system. The sensory feedback is from the motion states of the walker to both the neural signal controller and the coupled neural oscillator.

and the interaction between the mechanical system and environment. The architecture is shown in Fig. 2. The performance of different walking patterns is evaluated by velocity and step frequency, which is equivalent to velocity and step length, since frequency is the ratio of velocity to step length. Different from most previous studies which controlling only the speed, the CPG model in this paper is expected to control both velocity and step length simultaneously. Thus the walking behavior can be modulated over a wide range by controlling natural dynamics.

The control system consists of the neural signal controller and the coupled neural oscillators. The neural signal controller generates appropriate signals u_e and u_s according to the desired walking pattern and the actual walking performance. The signals, for setting the level of activity of the neural coupled oscillators, can be compared to the stimulation from the brain activating the spinal cord of many vertebrate animals [22]. The two parameters u_e and u_s are responsible for adjusting the equilibrium positions and the stiffness of each joint, respectively. The coupled neural oscillators receive input signals u_e and u_s and output rhythmic patterns of joint torques and joint stiffness, to generate periodic stable gaits. The control system contains twelve unit oscillators, associated with walking phase-dependent sensory feedback from the motion states (i.e. the generalized coordinates and velocities) and foot contact information. Each joint is controlled by two unit oscillators, producing the equilibrium position and stiffness respectively.

Inter-limb coordination of the two legs are established between the hip unit oscillators on the contralateral side. Inhibitory connection of equilibrium positions results in phase difference between hip angles and thus form periodic motion, while the stiffness of the two hip joints are positively correlated by the coupling. Intra-limb coordination makes the stiffness of ipsilateral joints increase or decrease proportionally. Derivative feedbacks of hip and ankle angles are added to the coupled neural oscillators for decreasing time delay effects and preventing the limb moving too fast to maintain stable walking. The unit oscillator for controlling equilibrium position of the knee joint of the swing leg receives feedback from the amount of foot clearance. The knee torque of the swing leg adapts to the current leg posture to avoid foot scuffing by as low energy consumption as possible. The unit oscillator for ankle stiffness of the stance leg receives sensory feedback from the ankle joint angle and angular velocity. The stiffness increases adaptively in dorsiflexion, which is consistent with the general tendency of human normal walking [23]. All these principles of feedback mentioned above are appropriate for different gaits, velocities and step lengths. Thus flexible walking pattern transitions can be realized by just tuning u_e and u_s.

2.3 Human Walking Experiments

For the validation of the proposed model, we observed human motion at constant and varied velocities and recorded the kinematic data. Five subjects (five males, 24.4 ± 3.0 years old, $1.7m \pm 0.07m$ height, $69.60kg \pm 3.97kg$ weight) were asked to walk uniformly at the natural speed, a smaller speed and a larger speed respectively. Then they performed walking pattern transitions from a slow gait to a fast gait in three manners as following:

1) Method 1: The subjects increase their walking speeds mainly by adjusting the step lengths, while the step frequency has only a small change;

2) Method 2: The speed transitions are realized in the self selected way;

3) Method 3: The subjects increase their speeds mainly by adjusting the step frequency, while the step length has only a small change.

We placed notice lines on the ground to help the subjects adjust the step lengths. The human motion data were obtained by Codamotion (Charnwood Dynamics Ltd.). The speed, step length and joint trajectories were represented by the average values and the standard deviations over all the subjects, as shown in the following section.

3 Results

In this section, we display both the simulation results and human motion results. The walking performance of the proposed model and human motion are compared.

3.1 Steady-State Walking

Different stable walking patterns are obtained by adjusting joint torques and joint stiffness of our model. Fig. 3 and Fig. 4 indicate the joint trajectories of cyclic motion with

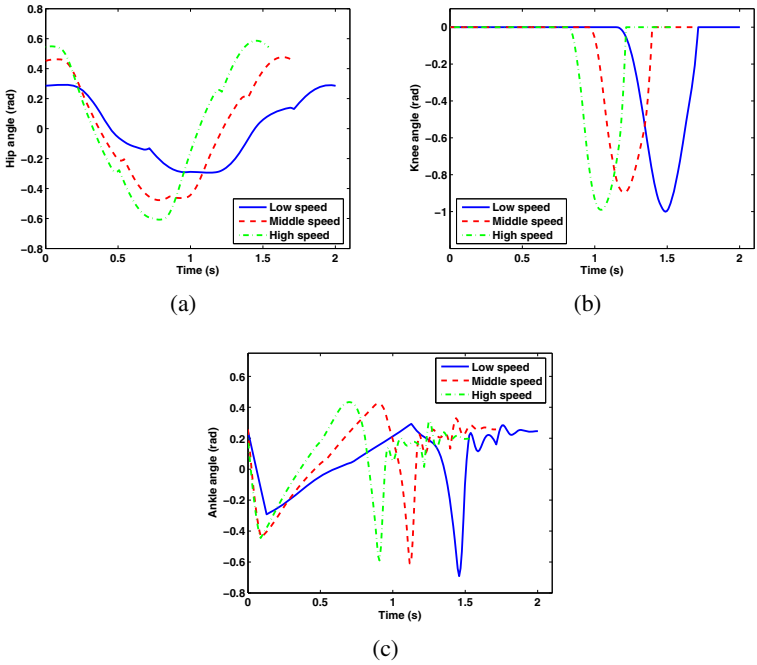

Fig. 3. Joint trajectories of different speeds of the proposed model. (a), (b) and (c) are hip angle, knee angle and ankle angle respectively. The blue solid line, the red dashed line and the green dot-dashed line represent the motions at $0.46m/s$, $0.83m/s$ and $1.15m/s$ respectively.

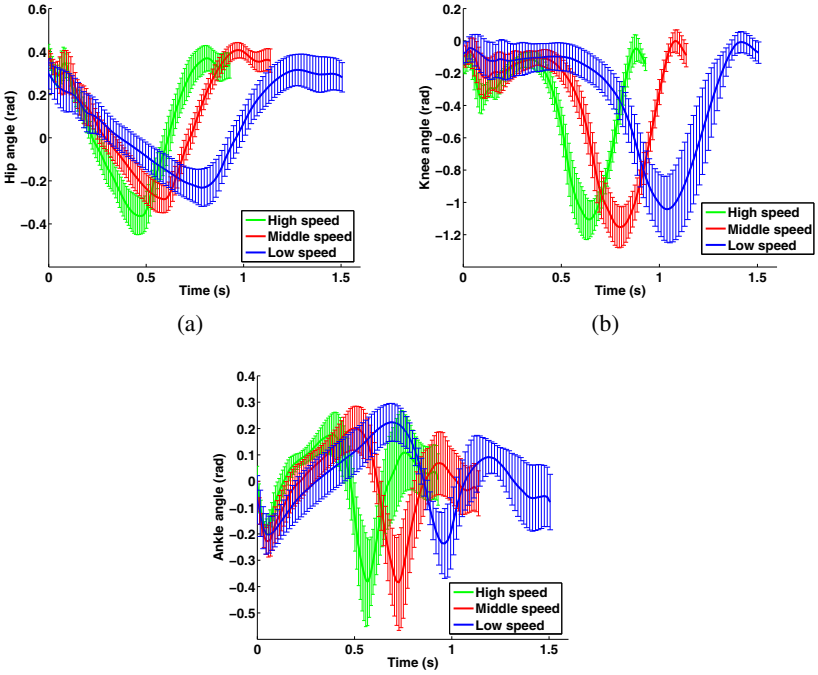

Fig. 4. Joint trajectories of different speeds of human walking. (a), (b) and (c) are hip angle, knee angle and ankle angle respectively. The blue solid line, the red dashed line and the green dot-dashed line represent the motions at $0.61 \pm 0.15m/s$, $0.98 \pm 0.15m/s$ and $1.40 \pm 0.29m/s$ respectively.

different speeds of the proposed model and human motion, respectively. The speeds of the selected motion patterns of the simulation model are $0.46m/s$, $0.83m/s$ and $1.15m/s$, respectively. The corresponding Froude numbers (defined as $Fr = V/\sqrt{gl}$, where V is the velocity, g is the gravitational acceleration and l is the leg length) are $0.16, 0.30$ and 0.41 respectively as the leg length is $0.8m$. In human motion experiments, the walking speeds of different walking patterns are $0.61m/s \pm 0.15m/s$, $0.98m/s \pm 0.15m/s$ and $1.40m/s \pm 0.29m/s$, respectively (represented as the mean value of different subjects $\pm$ the standard deviation). The corresponding Froude numbers are 0.21 ± 0.05, 0.33 ± 0.04 and 0.47 ± 0.09, respectively, which are a little larger than the speeds of the simulation model.

Both the two types of results show similar tendencies. Larger speed leads to smaller step period and larger amplitude of hip angle. The flexion of the knee joint becomes earlier with increasing speed. The ankle angle trajectory of the model performs more obvious oscillation in swing phase than that of human motion, for the joint stiffness is modeled as a torsional spring in the proposed model. In general, the joint trajectories of our model are close to those of human motion, which demonstrates that our model

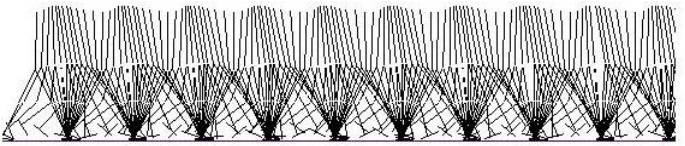

Fig. 5. The stickgram of stable walking at $0.83m/s$ of the bipedal walking model with adaptable stiffness joints and the CPG-based control method

can generate natural bipedal walking performance and reflect the motion characteristics over different speeds. Fig. 5 shows the walking trajectory of the proposed bipedal model at a speed of $0.83m/s$.

3.2 Walking Speed Transition

Since the proposed bipedal model has adaptable joint stiffness and controllable joint torques, real-time walking pattern transitions can be achieved. Adding adaptable joint stiffness to the CPG-based model makes it possible to control speed and step length (or step frequency) independently. Therefore, we show walking speed control with different step frequency behaviors.

In simulation, the speed is changed from $0.56m/s$ to $1.0m/s$ by adjusting control parameters on-line. The initial step frequency is $1.06Hz$ (thus the initial step length is $0.53m$). We applied three different methods to the speed transition. The target step frequencies are $1.12Hz$, $1.20Hz$ and $1.26Hz$ in method 1, method 2 and method 3, respectively. Therefore, the corresponding target step lengths are $0.89m$, $0.83m$ and $0.79m$ respectively. These three methods are accordance with the three pattern transition methods in human motion experiments mentioned in the previous section. The portions of step length variation and step frequency variation are different in different methods.

Fig. 6(a) shows the speed transitions of the three methods of the simulation model. All the methods have acceptable control precision since the final speeds are close to the desired value. The rise time of speed variation in method 1 is shortest, which indicates that walking performance is more sensitive to step length variation than to step frequency variation. Adding joint stiffness control can improve the control accuracy. Fig. 6(c) represents the changes of step lengths of the bipedal model in the three methods. One can find that the step lengths of different methods achieve different steady-state values with almost the same speed change trend. Thus adding adaptable stiffness can realize more precise walking pattern control and obtain multiple speed transition manners. Fig. 7 shows the walking trajectory of speed transition in method 2.

The speed transitions in human locomotion also show similar trends. In different methods, the subjects achieve almost the same ultimate speeds while obviously different step lengths. When the change of step length plays a primary role, the final step length will reach a relatively large value (as shown in method 1 of Fig. 6(d)). Contrarily, if the speed transition is caused mainly by the change of step frequency, the final step length will stay at a low level and the subject will increase the speed mainly by increasing the step frequency. Comparison of hip angle trajectories of the proposed model and human

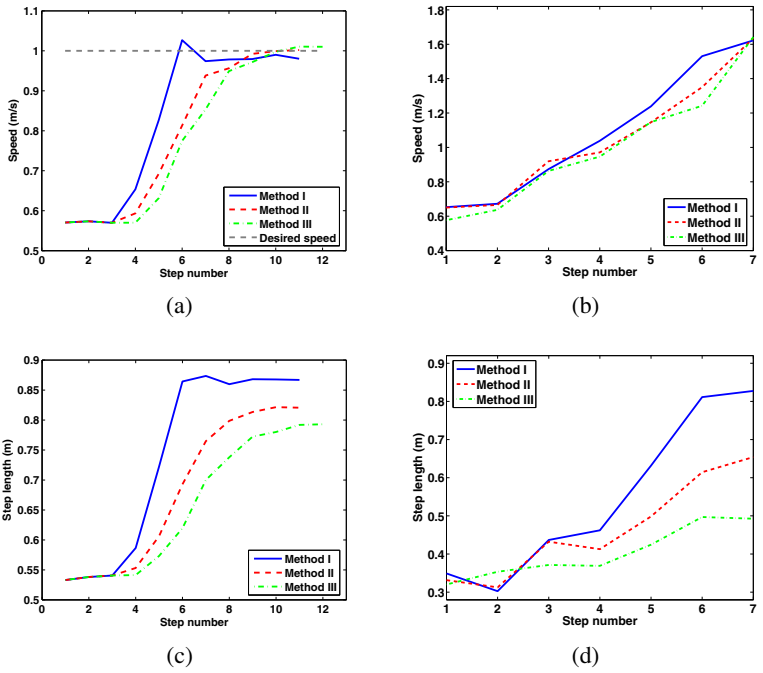

Fig. 6. Comparison of speed transitions of the proposed bipedal model and human walking. (a): speed variation of the model. The gray dashed line represents the desired speed. (b): speed variation of human walking. (c): step length variation of the model. (d): step length variation of human walking.

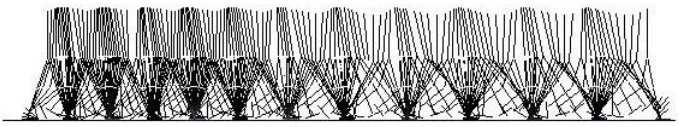

Fig. 7. The stickgram of speed transition of bipedal walking model with adaptable stiffness joints and the CPG-based control method. The initial speed is $0.56m/s$ and the ultimate speed is $1.0m/s$. The step length is changed from $0.53m$ to $0.83m$.

locomotion is illustrated in Fig. 8. The hip angle curve of method 3 has a small rise in amplitude and a large increment in frequency, while method 1 has the largest final amplitude, which corresponds to the largest final step length. Similar results can be observed in human locomotion. Comparison of the results from the simulation model and from human locomotion experiments indicates that the proposed model can explain different manners of speed transitions in human walking.

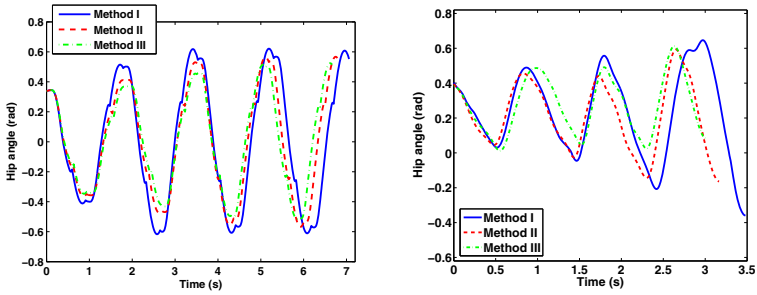

Fig. 8. Comparison of hip angle trajectories during speed transitions of the proposed bipedal model and human walking. (a): hip angle trajectories in three methods of the bipedal model. (b): Hip angle trajectories in three methods of human walking.

4 Conclusion

In this paper, we established a passivity-based dynamic bipedal walking model with an upper body, compliant knee and ankle joints, and flat feet. A bio-inspired CPG-based method is applied to the motion control. In addition, we add adaptable joint stiffness to the locomotor system. To validate the effectiveness and the natural performance of the model, we carried out simulation experiments and human motion experiments. Simulation results show that stable motion cycles with different walking speeds can be achieved in the proposed model. Comparison of the results from simulations and from human motion experiments indicates that human-like walking pattern transitions and multiple speed control methods can be realized by adding joint stiffness control. The model can reproduce natural bipedal locomotion, help better understand the principles of real human walking, and provide a new solution of building efficient bipedal robots with natural gaits.

To extend the study in this paper, we intend to improve the method to raise the control accuracy, and apply the idea of the proposed bipedal model to a physical prototype in the future.

Acknowledgements. This work has been funded by National Natural Science Foundation of China (No. 61005082, 61020106005) and the 985 Project of Peking University (No. 3J0865600).

References

1. Hirai, K., Hirose, M., Haikawa, Y., Takenaka, T.: The development of the Honda Humanoid robot. In: Proc. of the IEEE Int. Conf. Robotics and Automation, Leuven, Belgium, pp. 1321–1326 (1998)
2. McGeer, T.: Passive dynamic walking. Int. J. Robot. Res. 9, 68–82 (1990)
3. Collins, S., Ruina, A., Tedrake, R., Wisse, M.: Efficient bipedal robots based on passive-dynamic walkers. Science 307, 1082–1085 (2005)

4. Wisse, M., Hobbelen, D.G.E., Schwab, A.L.: Adding an upper body to passive dynamic walking robots by means of a bisecting hip mechanism. IEEE Trans. Robot. 23(1), 112–123 (2007)
5. Borzova, E., Hurmuzlu, Y.: Passively walking five-link robot. Automatica 40, 621–629 (2004)
6. Kwan, M., Hubbard, M.: Optimal foot shape for a passive dynamic biped. J. Theor. Biol. 248, 331–339 (2007)
7. Wang, Q., Huang, Y., Zhu, J., Wang, L., Lv, D.: Effects of foot shape on energetic efficiency and dynamic stability of passive dynamic biped with upper body. Int. J. Humanoid Robotics 7(2), 295–313 (2010)
8. Hobbelen, D.G.E., Wisse, M.: Controlling the walking speed in limit cycle walking. Int. J. Robot. Res. 27(9), 989–1005 (2008)
9. Wang, Q., Huang, Y., Wang, L.: Passive dynamic walking with flat feet and ankle compliance. Robotica 28, 413–425 (2010)
10. Huang, Y., Wang, Q., Chen, B., Xie, G., Wang, L.: Modeling and gait selection of passivity-based seven-link bipeds with dynamic series of walking phases. Robotica 30, 39–51 (2012)
11. Vanderborght, B., Van Ham, R., Verrelst, B., Van Damme, M., Lefeber, D.: Overview of the lucy project: dynamic stabilization of a biped powered by pneumatic artificial muscles. Adv. Robotics 22(10), 1027–1051 (2008)
12. Ishikawa, M., Komi, P.V., Grey, M.J., Lepola, V., Bruggemann, G.: Muscle-tendon interaction and elastic energy usage in human walking. J. Appl. Physiol. 99, 603–608 (2005)
13. Hobbelen, D.G.E., Wisse, M.: Ankle actuation for limit cycle walkers. Int. J. Robot. Res. 27(6), 709–735 (2008)
14. Owaki, D., Osuka, K., Ishiguro, A.: On the embodiment that enables passive dynamic bipedal running. In: Proc. of the IEEE Int. Conf. Robotics and Automation, Pasadena, CA, USA, pp. 341–346 (2008)
15. Huang, Y., Vanderborght, B., Van Ham, R., Wang, Q., Van Damme, M., Xie, G., Lefeber, D.: Step length and velocity control of a dynamic bipedal walking robot with adaptable compliant joints. IEEE-ASME Trans. Mechatron. 18, 598–611 (2013)
16. Taga, G., Yamaguehi, Y., Shimizu, H.: Self-organized control of bipedal locomotion by neural oscillators in unpredictable environment. Biol. Cybern. 65, 147–159 (1991)
17. Verdaasdonk, B.W., Koopman, H.F.J.M., van der Helm, F.C.T.: Energy efficient walking with central pattern generators: from passive dynamic walking to biologically inspired control. Biol. Cybern. 101, 49–61 (2009)
18. Owaki, D., Kano, T., Tero, A., Akiyama, M., Ishiguro, A.: Minimalist CPG model for inter- and intra-limb coordination in bipedal locomotion. In: Lee, S., Cho, H., Yoon, K.-J., Lee, J. (eds.) Intelligent Autonomous Systems 12. AISC, vol. 194, pp. 493–502. Springer, Heidelberg (2013)
19. Amemiya, M., Yamaguchi, T.: Fictive locomotion of the forelimb evoked by stimulation of the mesencephalic locomotor region in the decerebrate cat. Neurosci. Lett. 50, 91–96 (1984)
20. Cazalets, J.R., Borde, M., Clarac, F.: Localization and organization of the central pattern generator for hindlimb locomotion in newborn rat. J. Neurosci. 15, 4943–4951 (1995)
21. Ijspeert, A.J.: Central pattern generators for locomotion control in animals and robots: a review. Neural Netw. 21(4), 642–653 (2008)
22. Grillner, S., Georgopoulos, A.P., Jordan, L.M.: Selection and initiation of motor behavior. In: Stein, P.S.G., Grillner, S., Selverston, A., Stuart, D.G. (eds.) Neurons, Networks and Motor Behavior. MIT Press (1997)
23. Frigo, C., Crenna, P., Jensen, L.M.: Moment-angle relationship at lower limb joints during human walking at different velocities. J. Electromyogr. Kines. 6, 177–190 (1996)